Dynamics of non-dense sodium silicate - water system studied by molecular dynamics

Malgorzata Kaminska, Frédéric Gruy, Jules Valente

Dynamics of non-dense sodium silicate - water system studied by Molecular Dynamics

Małgorzata Kamińska [a,b], Frédéric Gruy [a](*), Jules Valente [b]

a - Mines Saint-Etienne, Univ Lyon, CNRS, UMR 5307 LGF, Centre SPIN F - 42023 Saint-Etienne France

b - Solvay, RIC Paris, 52 rue de la Haie Coq, F - 93308 Aubervilliers France

* corresponding author

gruy@emse.fr

0033477420202

ABSTRACT

A wide range of applications of amorphous silica makes this mineral an object of various investigations conducted by the scientists and the industry. The procedure of its precipitation is well studied, and we dispose of a range of models describing the succeeding processes. However, the size restrictions of experimental methods limit the knowledge about the very first instants of the process. Therefore, to contribute to filling this gap, our study aimed at elucidating some aspects of silica oligomerization. To access the molecular details of the process, we applied the Molecular Dynamics method with the ReaxFF Reactive Forcefield. We studied sodium silicate solutions with high initial concentration. We took up the topic of the effect of temperature, the size of the simulated system, and the amount of water in the simulations. Our considerations led us to conclusions about the reaction mechanism. We applied this knowledge to propose later a simple model describing the evolution of small species. Finally, we estimated the corresponding kinetic constants, which explained well the succession of events and reasonably agreed with the theory.

Keywords: sodium silicate, oligomerization, molecular dynamics, mechanism, kinetic constant values

Introduction

Precipitated silica, with its application in many branches of the industry – rubber, agrochemical, ceramics, oral care, food and feed, among others, has gained popularity in recent years. Thus, nowadays, we dispose of a vast amount of data concerning the growth of silica particles, their aggregation, and agglomeration, as well as the dependence of those steps on experimental conditions [1], [2]. However, we have not yet reached a full understanding of the process. We still need to shed some light on the very first instants of silica precipitation, just after the neutralization of the sodium silicate solution, when the system transformations lead to the formation of silica nanoparticles. Bridging this gap is crucial for full control over the final product morphology.

If we look into the experimental studies on silica polycondensation, we see that the researchers implemented a spectrum of methods, including silico-molybdate method [3]–[6], ^{29}Si Nuclear Magnetic Resonance [7]–[11], Dynamic Light Scattering [5], [6], [11], Static Light Scattering [5], [6], [12] Small-Angle X-ray Scattering [7], [9]–[11], Fourier-Transform Infrared Spectroscopy [8] and Transmission Electron Microscopy [13]. In the majority of the cases, they employed a combination of two (or more) experimental techniques to ensure their mutual verification and access to complementing data. The obtained results allowed the researchers to speculate on the reaction mechanism and the impact of experimental conditions on the condensation of silicates.

The well-established theory is that nucleation is an abrupt process, requiring a supersaturation high enough to launch the reaction [14]. The early beginnings of the reaction, consisting of spontaneous, overlapping processes, lead to the generation of a variety of small oligomers [15]. These species, then, transform further via reactions including cyclization (i.e., internal reorganization of species), monomer addition to larger clusters, and cluster-cluster collisions. What is the sequence of events in the evolving species? Is there a specific moment in the system evolution when the clusters (of a specific size?) are more prone to reorganize rather than to react with other species? Those questions stay open while the authors provide contradicting theories.

An interesting example is the determination of the rate-limiting, i.e., the slowest step of the whole process. According to Rothbaum and Rohde [16], it is dimerization. This hypothesis does not coincide with the results of other authors, previously evoked [14], [15], who claim that the neutralization of silicates leads to the instantaneous formation of a mixture of small species, including dimers, but not limited just to those species.

The discrepancies found in the literature, point to another widely evoked problem, which is the impact of the operational conditions on the precipitation process. One of the most critical parameters is the temperature of the reaction mixture. It accelerates the reactions, leading to a much faster system evolution [17], [18]. Nonetheless, some contradictory experimental results question this simple dependency, stressing the role it plays in setting the initial supersaturation [3],

[16], [19]. Another crucial factor is the pH of the solution. The majority of studies report on the accelerating effect of implementing a higher pH on silica condensation [3], [20]–[22] (pH>3). It is explained as a consequence of the presence of hydroxyl ion, promoting polymerization. Finally, silica concentration, which sets the initial supersaturation, and influences the reaction rate, plays a significant part in the process. Several researchers evoked the positive effect of raising the initial concentration on shortening the induction period (i.e., the time interval before the reaction can be experimentally detected) and accelerating the condensation process [3], [14], [16], [20], [23], [24].

The experimental studies on the kinetics of the beginnings of silica precipitation mention the induction period, followed by the processes put together (in the majority of the cases) into one group classified as "silica condensation". The origin of such simplification lies in the detection limits of experimental methods, which are not able to access the sub-nanometer scale of oligomerization. Consequently, they cannot make a distinction between the early oligomerization reactions. Furthermore, quite possibly, those reactions are not even detected, as they fall in the "induction time" period. Hence, there is a demand for methods providing access to the molecular details of the processes of interest.

Molecular Dynamics is a computational method employed to simulate the temporal evolution of the systems at predefined conditions. Solving the equations of motions allows calculating (at each iteration) the positions and velocities of all the atoms in the system. Simultaneously, the reactive potential, with experimental parameters trained for the specific system, account for the interactions between the atoms, including the formation and breakage of bonds. Consequently, we can follow the morphology of clusters evolving from a given initial mixture of molecules. We can, therefore, extract information about the reaction mechanism, the succession of events, and even speculate about the kinetics of such system transformations.

The literature provides several examples of MD simulations on the evolution of silicate species. In essence, we can separate such studies into three main groups. The first one implements the Garrofalini-Feuston potential [25], [26]. This interatomic potential is straightforward, and it does not account either for charge transfer or polarizability. It is, however, the subject of a few studies [27], [28], each of which expanded the system size and reached further simulations steps. The most noteworthy is the research published in 2004 by Rao, who detected in their simulations a cluster of 6.72 nm in length. This species was very elongated and not dense enough to call it a critical cluster or a particle (the possible cause is the primitive reactive potential), but, still, to the best of our knowledge, it is the largest nucleus detected in MD simulations on silicates. This nucleus appeared in the simulation of Rao at a very high temperature of 2500K (to accelerate the reactions) after 12.5ns of simulation time.

The second group of methods implements Car-Parrinello Molecular Dynamics - a technique derived from a combination of Density Functional Theory and MD simulations. This method, much more precise, does not allow reaching advanced simulation times. Trinh et al. [29] and

Pavlova et al. [30] focused on the very first instants of the synthesis of zeolites. The former research included small oligomers up to tetramers, while the later limited the study to dimers and trimers. They both concentrated their efforts on determining the reaction mechanism by studying the species privileged within the considered range. Pavlova also included the effect of the presence of Na^+ ion, concluding on its repressing impact on dimerization and trimerization. They assigned this finding to the rearrangement of hydrogen bonds of water surrounding reacting species, forced by sodium.

The third family of MD simulations includes the reactive ReaxFF potential, developed by van Duin et al. [31]. We can find two examples of such a study – the one of Jing et al. in 2015 [32] and the more recent study of Du et al. in 2018 [33]. Jing implemented the replica-exchange method to apply the realistic temperatures in their study of the beginning of the zeolite synthesis (353-543K). Their investigation with the water-to-silicon ratio of 5 (300 H_2O and 60 $Si(OH)_4$ molecules), allowed them to study the evolution of the system, leading to the formation of a cluster built of ~30 Si atoms. They studied the role of sodium ion and temperature on oligomerization reactions. They noticed that sodium was promoting faster oligomerization: the effect was strong at lower temperatures, and became less significant with the rise in temperature.

Then, Du et al. examined the systems with the water-to-silicon ratio of 0-9 and the temperature in the range of 1500 to 3000K. Those simplifying and accelerating factors allowed them to study the effect of the applied forcefield. They compared the forcefield of Fogarty et al. [34] and Yeon et al. [35]. Interestingly, even if they did notice that the reaction was launched sooner with the forcefield of Fogarty, the final equilibrium state did not vary in the two cases. Du et al. also examined the impact of temperature, stating the accelerating effect of the rise in temperature on the condensation ratio. They estimated the activation energy of 109kJ/mol for the forcefield of Fogarty and 160kJ/mol for the forcefield of Yeon. Then, they calculated the polymerization rate. Extrapolation to 300K provided them with a value of $0.016min^{-1}$ and $0.003min^{-1}$ for the water-to-silicon ratio of 0 and 3, respectively. Next, examining the technical aspects of their simulation, they observed that in the smaller system (N_0=64 as compared to N_0=512; T=2000K, n_{HS}=3; N_0 is the number of silicon atom inside the simulation box, n_{HS} denotes the water-to-silicon ratio), the polymerization rate is slightly higher, and the number of species fluctuates more. Subsequently, they proved that increasing the amount of water was resulting in a decrease in the final condensation ratio and an increase in the activation energies.

As explained, Molecular Dynamics simulations found in the literature are, in the majority of the cases, limited to the very first instants of the process. Furthermore, they do not provide a consistent reaction mechanism. Even the conclusions on the effect of operating conditions are not mutually consistent. Therefore, we wish to provide a study collecting the impact of operational conditions and technical aspects of simulations. The current investigation focuses on elucidating the reaction mechanism, developing a corresponding model, and estimating the values of kinetic constants. To reach longer simulation time, we apply the simplification evoked in the literature

(f.ex., [28], [32], [33]), applying a lower water content. In some of our investigations, we also accelerate the reactions, implementing a high temperature. Focused on the industrial method used for silica precipitation, we chose to work at a basic pH and a silicate concentration resembling a realistic one. Therefore, we investigate solutions with an initial silicate concentration, C_0=115gSiO_2/L, evolving at pH=9.8.

The paper is organized as follows. Section 2 includes a description of materials and methods based on Molecular Dynamics. Section 3 presents some results comprising the effect of the system size, temperature, and water-to-silicon ratio on the oligomers morphology and the oligomerization kinetics. In section 4, we discuss those results, proposing a mechanism of oligomerization, corresponding to the operating parameters in the considered range. Section 5 concludes the paper.

1 Materials and methods

Our study used the SCM implementation of ReaxFF reactive potential [31], [36], [37] with the forcefield file from Rahnamoun et al. [38] (Si/O/H/Na interactions). We ran the simulations on the computational cluster (facility) of École des Mines de Saint-Étienne, 'Centaure', composed of 28 computing nodes with a total of 560 cores and 1.8 TB of RAM. The average execution time for computation of 0.5ns simulation time for one of our systems, using 1 node (28 cores), was 7 to 10 days.

First, before each simulation, we packed the molecules into the simulation box with periodic boundary conditions. We set the number of molecules and the size of the box, determining the concentration, C_0. Our systems were composed of $Si(OH)_4$, $Si(OH)_3O^-Na^+$, and H_2O molecules. We set pH by changing the ratio of the number of $Si(OH)_4$ to $Si(OH)_3O^-$ molecules as follows the equation (pKa_1=9.8)

$$\mathrm{pH} = \mathrm{pKa_1} + \log([\mathrm{SiO(OH)_3^-}]/[\mathrm{Si(OH)_4}]). \quad (1)$$

We attempted to repeat each simulation three times. However, in some cases (especially at higher temperatures), our simulations stopped prematurely because of the system's destabilization. Thus, we dispose of either three (the majority of simulations) or only two, one or even none repetitions. Regardless of how many simulations we had, we then calculated the average number of species coming from all the trials. Subsequently, we calculated average for every forty time steps to smooth the data series and to limit the system fluctuations.

The choice of the simulation parameters

As mentioned before, preparing simulations started by setting the initial number of all molecules. We set the pH to 9.8 with $nSi(OH)_4/nSi(OH)_3O^-Na^+=1$. The majority of our simulations included 64 monomers. We justified this choice, testing different system sizes, implementing N_0=64, 216, and 500 (N_0 – initial number of monomers).

The most significant simplification we made was applying a limited amount of water to ensure (relatively) fast system evolution. This "shortcut", already applied by other researchers, allowed us to perform a vast number of simulations (120 without the repetitions) and to study a spectrum of technical and experimental conditions. We, therefore, studied systems with n_{HS} = 0, 0.5, 1, and 2 (where n_{HS} is the ratio between the number of water molecules and the number of silicon atoms).

The impact of N_0 and n_{HS} on the system evolution is one of the subjects of section 3.

To set the concentration, we, then, chose the size, a, of the box. We tested the initial concentration, C_0=115gSiO_2/L (a= 38.2Å for N_0=64), which is an experimentally realistic (but relatively high) concentration, which we then compared with an even higher concentration of 342 gSiO_2/L (a=26.57Å for N_0=64). As expected, increasing the initial concentration resulted in a much more abrupt system evolution, accelerating the reactions by decreasing distances between the reacting molecules. However, the concentration of 342gSiO_2/L is not realistic, and the obtained results present higher fluctuations than at the lower concentration, masking the real tendencies. Thus, in the current investigation, we focus on C_0=115gSiO_2/L.

The position of molecules in the simulation box was, in the vast majority of the cases, randomized. We performed some tests with a deterministic placement of species, locating them on a predefined grid. The only difference we noticed was a delicately more abrupt start of condensation for randomly placed molecules with the results of both series coinciding after ~0.005ns.

Having prepared the system, we then chose the technical aspects of simulations. We decided to set the simulation step of 0.25fs (a time step fast enough to cover the fastest changes in the reactive system), and the Bond Order cutoff of 0.3 as done by other authors (f.ex., [32]).

In our investigations, we examined the effect of temperature on silica condensation. Thus, we chose a wide range of values, starting with realistic 300K and, then, raising it to 600, 1000, 1500, and finally, 2000K. The problem we encountered at the highest temperatures was the destabilization of the reactive system (too high velocities of molecules), which was causing a premature stop of some of our simulations. To avoid this problem, we implemented 10^4 non-reactive iterations before the "actual" simulations. We compared the evolution of such systems with the systems without the prior pre-equilibration, and we stated that the results coincide. That allowed us to prepare more stable systems, which were less prone to provoke the simulation crush. However, this method, as already mentioned, did not prevent errors in each case.

Finally, we set the simulation time. We chose 0.5ns, which led to relatively advanced system evolution. It was the case in each of our simulations unless the previously evoked errors prevented the simulation completion.

2 Results

In this section, we present an analysis of the evolution of the system in simulation time. To compare the results, we represent them as a normalized number of species, dividing the number of the clusters of a given size by the initial number of monomers, N_0.

The effect of N_0

First, we compared the results of simulations for different system sizes for the systems without water (N_0=64 or N_0=216) and with water (where n_{HS}=0.5; N_0=64/68, N_0=216, or N_0=500). Figure 1 presents the results of the former. We chose this simulation for clarity reasons; the results juxtaposed in both cases. As we can see from the (normalized) evolution of species with simulation time, the size of the simulated system does not seem to play a significant role. What we can notice is slightly higher fluctuations in the case of smaller systems, but the results coincide well.

The morphology of evolving systems

Then, we examined the structure of clusters randomly chosen at different time instants, to gain a general idea about the morphology of evolving systems. Table 1 sums up the results of such analysis. Figure 2 shows an example picture of silicate species.

In general, in the whole range of temperatures (300-2000K), for all of the n_{HS} values tested (0-2), we noticed that the species tend to assemble very soon after the beginning of the simulation. We, then, quite quickly detect the species $Si_{n>1}$. Those clusters consist of silicate anions connected by a Na^+- Na^+ linkage with a Bond Order >0.4. In the case of larger species, Na^+ forms a net-like structure. Interestingly, at 600K, we detected the largest cluster, containing 13 silicon atoms.

Another type of bond detected is a hydrogen bond, linking silicates with a molecule of water, sodium hydroxide, or neutral monomer. Consequently, we could state that the detected clusters are not oligomers, i.e., they do not have the Si-O-Si covalent bond. We could instead classify them

as aggregates. Furthermore, the vast majority of the detected aggregates did not contain the neutral $Si(OH)_4$, but rather the anionic $Si(OH)O_3^-$ monomeric species.

However, at 1500K after 0.35ns, we did detect a covalent Si-O-Si bond. We should stress here that our simulations at 2000K stopped prematurely. Thus, 1500K was the highest temperature for which we reached an advanced simulation time, and, in this case, we can say that we observed a typical structure of silicate oligomer.

We should remind the reader that we performed our analysis at specific time instants, so we dispose of a few sampled pictures extracted from the simulations. Hence, our results are highly dependent on the system fluctuations, and a more in-depth analysis of the events of interest would require applying more sophisticated computational tools. With this remark, we now move to the discussion on the effect of T and n_{HS} on the system evolution.

The role of temperature in the system evolution

We can deduce the effect of temperature, based on Figure 1, Figure 3, and Table 1. Looking at the figures, we can notice that the reaction starts more abruptly at lower temperatures (300, 600, and 1000K). Then, at T=300, 600, and 1000K, we observe a plateau representing an equilibrium state, reached within first ~0.1ns. At T=1500K, and 2000K, we observe more fluctuations, and the reaction is less advanced (those simulations stopped prematurely), which suggests that the system evolves further (the system has not yet reached an equilibrium). Those observations also suggest a shift in the reaction mechanism for T=1500K and 2000K, as compared to T=300, 600, and 1000K. This hypothesis seems probable, as we did observe different bond types in those two ranges of temperature when examining the morphology of the randomly-chosen clusters.

Furthermore, at 600K and 1000K, we can observe the presence of a minimum in the normalized number of monomers, which appears quite soon after the beginning of the simulation (~0.025ns). It was at those temperatures, as well, where we detected the largest clusters in the whole range of simulations, which together makes this subject worth a more in-depth analysis.

The effect of water-to-silicon ratio on system evolution

Figure 3 depicts the evolution of systems with different content of water. We compared n_{HS}=0, 0.5, 1, and 2. In the studied range of water-to-silicon ratios, temperatures, concentration, and the extent of simulations, we did not notice a significant effect of the content of water on the reaction. The corresponding data overlap, making it hard to make a distinction between them. The water-to-silicon ratio does not seem a key-parameter for explaining the behavior of the studied system.

We could note here that the size of the silicate species is ~0.5nm, and, at the studied concentration C≈2M, the average distance between two silicates is ~0.94nm. We can, therefore, state that the species are near each other. Furthermore, for n_{HS}=1, the distance between the centers of water molecules and silicate species is ~0.82nm, with water located close to silicate species. Nonetheless, the results of our MD simulations indicate that the role of water at those concentrations is negligible.

Note: Interestingly, the other authors, even studying a similar system and applying a similar method, mention 'polymerization' or 'oligomerization', when discussing their results. On the other hand, in our simulations, we observed mostly aggregation, with the formation of the covalent bonds appearing only at the highest temperatures and the most extended simulation times.

3 Discussion

System evolution at T= 600 and 1000K

The first feature which needs looking into is the system behavior at T=600K and 1000K. As a reminder, in Figure 1, we can notice the presence of a minimum in the normalized number of monomers, observed at 600K and 1000K. We do not make the same observation at T=300, 1500, and 2000K. At the same time, as we can see in Table 1, at T=600K, t_s=0.1ns, we detected a large cluster, built out of 13 Si atoms. It was the largest species detected during the sampling of the image series of the simulation box.

In Figure 4, we showed a typical particle size distribution (n_{HS}=1, N_0=64, T=600K, t_s=0.174ns) in the form of the mass concentration (proportion) as a function of cluster size. To smooth the resulting curve, we perform data averaging over a longer time-range (Δt=0.025ns) than the previous one ($\Delta t=10^{-4}$ns), recalculating the particle size distribution. In this figure, we can notice the presence of a peak for a large size. We observed that this large cluster appears at the time corresponding to the minimum in the normalized number of monomers vs. time (we do not show the corresponding data in this paper). We detected such oligomers for all N_0 studied. What is more, we stated that their size is proportional to N_0.

To better understand the succession of events corresponding to T=600K and 1000K, we revised the evolution of the system sizes in the simulations of interest. Then we compared the results for different values of N_0, n_{HS}, and T.

In the following part, we represent the results, as the mass proportion of the clusters of significant sizes ($N>N_0/8$), and the smaller species ($N\leq N_0/8$) in time.

Figures 5 and 6 show such a representation of the system evolution for various system sizes and water-to-silicon ratios, corresponding to different temperatures. Looking at those figures, we can see that the mass proportion of the larger clusters ($N>N_0/8$) is relatively independent of the content of water, and the system size.

At T=600K and 1000K, we notice the mass proportion of larger clusters is first rising with time (until ~0.15-0.20ns), and then (at ~0.20-0.23ns) we observe an asymptote. The particle size corresponding to the peak (detected for T=600K, and 1000K) is proportional to N_0 and corresponds to the presence of a single large species, built from $N_0/4$ - $N_0/5$ silicon atoms, which seems to stabilize with time. Small species surround this large cluster. Therefore, at longer simulation times, we observe certain extended properties in the sense of thermodynamics, since they are proportional to N_0. We can explain this observation, considering the equilibrium between the large cluster and the small species. We can deduce, from our MD simulations, the molar fractions of species coexisting at equilibrium. Table 2 reports these data. As we could expect, the molar fractions of small oligomers (Si_1-Si_4) are slightly higher at 1000K than at 600K (Table 2). At the same time, the nature of the equilibrium large cluster raises some questions. Its stability or quasi-stability, deduced from the fact that it does not dissolve, may suggest that it has already reached the critical size. We could, therefore, presume that the detected species is a pre-nucleus or a solid particle.

Reaction mechanism

Based on the considerations of the clusters' morphology and their size evolution, we propose the following reaction mechanisms, schematically represented in Figure 7.

T= 600K and 1000K

At 600K and 1000K, we observed some specificities which suggest the following succession of events: The first step is the formation of a mixture of small species of a size Si_1 - $Si_{N0/5}$; Then, a large cluster of a size $Si_{N0/5}$ - $Si_{N0/4}$ forms, already showing more stability than the smaller species. At the same time, smaller species drop in concentration; Next, the large cluster stabilizes, and the species of intermediate sizes dissolve; Finally, the system reaches equilibrium, in which one large cluster coexists with a mixture of small species of a size Si_1-Si_4.

T= 300K

At 300K, we did not detect the formation of the large cluster. However, we suspect that the system evolution is following the same steps as at 600K; the only difference is in the advancement of reaction. We assume that the system has only reached the first step within the studied simulation time.

T= 1500K and 2000K

The evolution of the system at the highest temperatures, should, logically, be the most advanced. However, it was not the case in our study. The reason for this unexpected tendency is the shift in the reaction mechanism, detected at those temperatures. We stated that the evolution of the system starts with the aggregation of small species, and then, we observe the formation of covalent bonds, proceeding, possibly, via the reorganization of already formed aggregates.

A method of quantitative analysis of the small clusters' dynamics ($Si_{N \leq 4}$)

To sum-up the obtained data, we followed with a quantitative examination of kinetics of the formation of small clusters.

First, to limit the number of adjustable values (kinetic constants), aiming at better accuracy and lower computational cost, we reduced the considered reactions to the formation of clusters up to Si_4 (we later explain the full procedure accounting for the conservation of the mass).

As a reminder, our initial solution contained molecules of $Si(OH)_4$, $Si(OH)_3O^-Na^+$, and H_2O. Having analyzed the system evolution and the morphology of the detected clusters, we assumed that the neutral silicic acid is non-reactive. To distinguish it from reactive anions, we denote it as Si_1^0. For the clarity reasons, we represent the clusters by the number of silicon atoms they consist of, and we omit other atoms (H, O, Na), proposing the following reaction scheme

$$Si_1 + Si_1 \overset{\vec{k_1},\ \overleftarrow{k_1}}{\longleftrightarrow} Si_2 \quad (2)$$

$$Si_1 + Si_2 \overset{\vec{k_2},\ \overleftarrow{k_2}}{\longleftrightarrow} Si_3 \quad (3)$$

$$Si_1 + Si_3 \overset{\vec{k_3},\ \overleftarrow{k_3}}{\longleftrightarrow} Si_4 \quad (4)$$

$$Si_2 + Si_2 \overset{\vec{k_4}}{\rightarrow} Si_3 + Si_1^0 \quad (5)$$

$$Si_2 + Si_3 \overset{\vec{k_5}}{\rightarrow} Si_4 + Si_1^0 \quad (6)$$

$$Si_2 + Si_2 \overset{\overrightarrow{k_6},\ \overleftarrow{k_6}}{\longleftrightarrow} Si_4 \quad (7)$$

$$Si_2 \overset{\overrightarrow{k_7}}{\rightarrow} Si_2' \quad (8)$$

$$Si_3 \overset{\overrightarrow{k_7}}{\rightarrow} Si_3' \quad (9)$$

$$Si_4 \overset{\overrightarrow{k_7}}{\rightarrow} Si_4' \quad (10)$$

Eq.2 represents the reaction between two monomers, and Eq.3 and 4 represent the addition of monomer to larger clusters. We consider those reactions to be reversible. The same stands for the collision of larger clusters, represented in Eq.7. Then, Eq. 5-6 represent the internal reorganization of clusters, which results in liberating a neutral silicic acid. This species is non-reactive, so this reaction is irreversible. Finally, Eq. 8-10 correspond to the formation (at T=1500K and 2000K) of the covalent bond, leading to the creation of an oligomer denoted as Si_N'. We assumed that oligomerization, being much slower than aggregation, results from the internal restructuring of species, as shown by Zhang [39]. We wish to emphasize that the introduction of steps 5 and 6 is the only way to explain the minimum in the temporal evolution of the number of monomers.

We then applied this simplified reaction scheme to estimate the kinetic constants (k_1-k_7). However, to ensure the conservation of the mass, we propose the following method for parameter estimation.

Due to the presence of the large cluster at T=600K and 1000K, the sum of the mass fraction of the four smallest clusters in the MD simulations is < 1, while we still want our mechanism, restricted to the four smallest clusters to follow the conservation of the mass. We, therefore, recalculated the MD-derived normalized concentrations, to which we fit our model. We followed the equation

$$C_{i,MD}'' = C_{i,MD} / \sum_{i=1}^{4} C_{i,MD} \,. \quad (11)$$

Note: We justify this simplification, pointing to the fact that $\sum_{i=1}^{4} i \cdot C_{i,MD} > 0.7$.

Next, we used a MATLAB script to estimate the kinetic constants k_1-k_7. We set the initial values for each kinetic constant and ran the optimization. To control the accuracy of the fitted values, we calculated the error

$$\mathrm{err} = \frac{1}{4}\sum_{i=1}^{4}\sqrt{\sum_{j=1}^{M}\left(C_{(i,j),\mathrm{Model}} - C_{(i,j),\mathrm{MD}}''\right)^2 \cdot \frac{1}{M}}\,, \qquad (12)$$

for the discretized time, j=[1,M].

We assumed a satisfying fit for err < 0.01 for the systems with (relatively) low fluctuations. At 1500 and 2000K, where the results fluctuated more, we accepted higher err (up to 0.022 in the worst cases).

Kinetic constants' values

Figure 8 shows the comparison of the MD-derived system evolution, corrected for the conservation of the mass with the data calculated from our simplified model. We can see that the fit is satisfying. Then, Table 3 reports on the estimated kinetic constants, including another representation of the accuracy – the calculated error.

If we look at the general tendencies, we can state that at T<1500K, the kinetic constants are little dependent on the size of the aggregate of interest and temperature. The constants of the direct reactions decrease only slightly when the temperature rises, while the reverse constants slightly increase. At the same time, the constants k_4 and k_5 corresponding to the restructuring of clusters, leading to the generation of neutral monomer, are high, suggesting a diffusion followed by fast restructuring.

The dynamics of the system concluded from the estimations made with our model agree well with the expectations. Now, to provide some justification for the obtained kinetic constant values, we should compare them with the theory.

The mean value of the kinetic constants of the direct reaction of aggregation is ~300 ns^{-1}. If we state the principles of our system dynamics, we see that what we observe could be described in the frame of the theory based on Eyring's pre-exponential factor [40], considering simple diffusion (without the formation of covalent bonds).

That leads us to the expression based on the Smoluchowski' collisional rate [41]

$$k_0 = 4\pi\left(D_i + D_j\right)\left(R_i + R_j\right)(N_A C_0), \qquad (13)$$

Then,

$$k_0 = 4\pi\left(\frac{k_B T}{2\pi}\right)^{1/2}\left(m_i^{-1/2} + m_j^{-1/2}\right)\left(R_i + R_j\right)(N_A C_0)^{2/3}, \qquad (14)$$

with $m_i = i \cdot m_1$ and $R_i = i^{1/3} \cdot R_1$.

i and j denote cluster sizes, m-mass, R-radius, D-diffusion coefficient, N_A-Avogadro's number.

Considering the reaction between a monomer and another species ($i=1$, $3 \geq j \geq 1$), we calculated the corresponding kinetic constant values. Table 4 reports on the estimated values.

As we can see, the kinetic constants depend little on the cluster size, decreasing only slightly for larger species. That tendency agrees with our observations.

However, the temperature plays a significant role ($k_0 \propto T^{1/2}$), which was not the case in our system. The calculated values do not coincide well either - the theory provides kinetic constants around five times higher than our model. The main reason for those differences is in the roots and the basics of the theory, not adjusted to concentrated solutions. Consequently, it does not account for the intermolecular interactions. The most straightforward correction of this theory would require adding a sticking efficiency factor (~0.2).

Alternatively, we can compute the diffusion coefficient of the species directly from k_0 and Eq.13. For instance, from monomer-monomer kinetic constant, the self-diffusion coefficient for the monomers is equal to $D_1 = 2 \cdot 10^{-8} m^2/s$ with $k_0 = 300 s^{-1}$ and $C_0 = 2M$; this corresponds to the order of magnitude of all diffusion coefficient values calculated from k_0 data in this paper. This value is higher than the diffusion coefficient of a molecule in liquid and much smaller than its diffusion coefficient in gas. This phenomenon is due to the high concentration of silicate species.

We introduce the Eq.14 to provide a reference value for k_0 having a physical sense. As a consequence, we do not expect this reference value to coincide with k_0 values coming from MD simulations. However, the estimated range of the reference and MD k_0 are similar. Without water ($n_{HS}=0$), the studied phenomenon is the self-diffusion. Kinetic theory of gases and Eyring theory, suitable for the non-dense system, lead to similar, but not identical, expressions for diffusion coefficients. Eq.14 results from Eyring's theory of diffusion. In the presence of a small amount of water ($n_{HS}<2$), the difference of mass between water and silicate species (appearing in the collisional events) leads to a small effect of water on diffusion constants.

Let us examine the thermodynamics of the $Si(OH)_4$ or $Si(OH)_3ONa$ system, i.e., possibly the final state of the non-reactive system after a long time. We expect that the interaction between $Si(OH)_4$ or $Si(OH)_3ONa$ molecules is stronger than the one between water molecules: Plyasunov [42] estimated the second virial coefficient of such $Si(OH)_4$ pairs and confirmed the strength of the interaction. Moreover, the size of the $Si(OH)_4$ molecule is known. Using the Van der Waals equation of state, we may estimate the critical parameters and the pressure in the system at a given temperature. Unfortunately, this computation is very sensitive to the co-volume value, and then, the result is only qualitative. However, we found a critical temperature (Tc=400-600K) close to the one of water, whereas the critical pressure (Pc=5-10 bar) is much smaller than the one of water. We have no such information for $Si(OH)_3ONa$ for which the raw data, e.g., the second virial

coefficient, are unavailable. However, we expect close critical parameter values for this chemical compound. From the values of the critical parameters and the investigated concentration-temperature range, the system would be in a supercritical fluid state if this assumingly non-reactive system would reach equilibrium. It is well known that the self-diffusion or mutual diffusion coefficients in a supercritical fluid are difficult to compute accurately; the corresponding values range between those in a gaseous and a liquid phase, which we observed in our case. Moreover, we wish to underline that we can obtain the self-diffusivity in a supercritical fluid from the kinetic theory of gases by multiplying the corresponding value by a factor depending on T/Tc and P/Pc ratio and ranging between 0.1 and 1 [43]. This approach is compliant with the introduction and the value of a sticking efficiency factor.

If we consider the reverse reactions, the value calculated based on elementary theory gives

$k_{0,i,reverse} = k_B T/h = 20840\ ns^{-1}$.

This value is much higher than our estimations, which we can explain by the slow breakage of the stable clusters following their restructuring.

On the other hand, at $T \geq 1500K$, the constants of the direct reaction (aggregation) are lower (half of the value for lower temperatures), with the constants of the reverse reactions similar to those at lower temperatures. The restructuring values drop, and the formation of covalent bonds appears. The kinetic constant of oligomerization-condensation reaction rises with an increase in temperature and water content. Its value is, nonetheless, low compared to other reactions.

The condensation reaction occurs at high temperatures, i.e., T=1500K and T=2000K. At T=1500K, the condensation rate is very low; therefore, the corresponding kinetic constant value is not accurate. Conversely, at T=2000K, the condensation rate is high and very sensitive to the water content. The water molecule catalyzes the formation of the Si-O-Si group. Uncertainty for kinetic constant values at T=1500K does not allow us to calculate the activation energy of the condensation reaction. At such small water content, the activation energy deduced from Arrhenius law is found within the range of 150-200 kJ/mol, whereas Du [33] has found an activation energy value equal to 109 kJ/mol and 160 kJ/mol depending on the forcefield used in their MD simulations of the condensation reaction in water as a solvent.

Again, the derived dynamics of the system seem reasonable.

4 Conclusions

In our Molecular Dynamics investigations, we studied the evolution of the systems with a small (or none) amount of water at different conditions. We focused on the effect of the system size (N_0=64, 216, 500), temperature (T=300, 600, 1000, 1500, and 2000K), and the amount of water (n_{HS}=0, 0.5, 1, 2) on the system evolution. We stated that the effect of the system size on the normalized number of species is negligible. Similarly, changing the water-to-silicon ratio did not affect the reaction in a significant way. The only parameter influencing (noticeably) the reaction was temperature.

Analyzing the morphology of evolving species, we stated that, at the temperatures in the range T=300-1000K, we only detected aggregates and no formation of covalent Si-O-Si bonds. Moreover, at T=600K and 1000K, we observed the presence of a minimum in the normalized number of monomeric species, corresponding to the formation of a large cluster and neutral monomers. At the same time at T=1500K, we observed some aggregates, and, after more advanced simulation time, we detected oligomers with covalent bonds. The simulation at 2000K stopped prematurely.

A more in-depth examination of the evolution of cluster sizes led us to the conclusion that at 600K and 1000K, we observe a four-step reaction mechanism. First, the small species of sizes Si_1 – $Si_{N0/5}$ start forming in the solution. Then, one large cluster of a size $Si_{N0/5}$ – $Si_{N0/4}$ emerges in the solution, and the concentration of small species drops. Next, the large species stabilizes, and the intermediate species dissolve. Finally, the system reaches an equilibrium, where the large, stable cluster coexists with smaller species, Si_1 – Si_4. We then discussed this equilibrium state and made a hypothesis based on the stable nature of the large cluster, stating that it might represent a pre-nucleus or a solid particle. However, determining with certainty the nature of this cluster's stability would require the analysis of the time evolution of the spatial structure of the oligomer in the simulation box**.**

We stated that the same reaction mechanism, limited, however, just to the first step, corresponds to the system evolution at 300K. At 1500 and 2000K, we observe the beginnings of aggregation and the formation of the covalent bonds.

To analyze the obtained results quantitatively, we proposed the simplified model, considering the formation of species up to Si_4, corrected to account for the conservation of the mass. The estimated values of kinetic constants suggest that, at T=300-1000K, we have relatively fast diffusion leading to the collision and aggregation of species. We demonstrated how our value of the kinetic constant of collision coincides with the Eyring's diffusion-aggregation theory, after applying a sticking efficiency factor of 0.2, to account for intermolecular interactions in concentrated systems. At those temperatures, we also observe a fast restructuring, followed by slower breakage of species.

Lastly, the values estimated for T=1500 and 2000K show that aggregation is much slower, and restructuring becomes a negligible phenomenon. At the same time, the formation of a covalent bond appears relatively slow as compared to diffusion.

Acknowledgments

The authors thank Solvay Company and the Agence Nationale Recherche et Technologie (CIFRE 2016-0186) for their financial support of this project.

5 References

[1] J. Schlomach and M. Kind, "Investigations on the semi-batch precipitation of silica.," *J. Colloid Interface Sci.*, vol. 277, no. 2, pp. 316–326, Sep. 2004, doi: 10.1016/j.jcis.2004.04.051.

[2] J. Valente, F. Gruy, P. Nortier, and E. Allain, "Evidence of structural reorganization during aggregation of silica nanoparticles," *Colloids Surf. Physicochem. Eng. Asp.*, vol. 468, pp. 49–55, Mar. 2015, doi: 10.1016/j.colsurfa.2014.12.006.

[3] A. Makrides, M. Turner, and J. Slaughter, "Condensation of Silica from Supersaturated Silicic-Acid Solutions," *J. Colloid Interface Sci.*, vol. 73, no. 2, pp. 345–367, 1980, doi: 10.1016/0021-9797(80)90081-8.

[4] D. J. Tobler, S. Shaw, and L. G. Benning, "Quantification of initial steps of nucleation and growth of silica nanoparticles: An in-situ SAXS and DLS study," *Geochim. Cosmochim. Acta*, vol. 73, no. 18, pp. 5377–5393, Sep. 2009, doi: 10.1016/j.gca.2009.06.002.

[5] M. Kley, A. Kempter, V. Boyko, and K. Huber, "Mechanistic Studies of Silica Polymerization from Supersaturated Aqueous Solutions by Means of Time-Resolved Light Scattering," *Langmuir*, vol. 30, no. 42, pp. 12664–12674, Oct. 2014, doi: 10.1021/la502730y.

[6] M. Kley, A. Kempter, V. Boyko, and K. Huber, "Silica Polymerization from Supersaturated Dilute Aqueous Solutions in the Presence of Alkaline Earth Salts," *Langmuir*, vol. 33, no. 24, pp. 6071–6083, Jun. 2017, doi: 10.1021/acs.langmuir.7b00887.

[7] M. T. Tognonvi, D. Massiot, A. Lecomte, S. Rossignol, and J.-P. Bonnet, "Identification of solvated species present in concentrated and dilute sodium silicate solutions by combined Si-29 NMR and SAXS studies," *J. Colloid Interface Sci.*, vol. 352, no. 2, pp. 309–315, Dec. 2010, doi: 10.1016/j.jcis.2010.09.018.

[8] L. Vidal *et al.*, "Controlling the reactivity of silicate solutions: A FTIR, Raman and NMR study," *Colloids Surf. -Physicochem. Eng. Asp.*, vol. 503, pp. 101–109, Aug. 2016, doi: 10.1016/j.colsurfa.2016.05.039.

[9] P. Wijnen, T. Beelen, and R. Vansanten, "Silica-Gels from Aqueous Silicate Solutions - Combined Si-29 Nmr and Small-Angle X-Ray-Scattering Spectroscopic Study," vol. 234, H. E. Bergna, Ed. Washington: Amer Chemical Soc, 1994, pp. 517–531.

[10] C. J. Y. Houssin *et al.*, "Combined in situ (29)Si NMR and small-angle X-ray scattering study of precursors in MFI zeolite formation from silicic acid in TPAOH solutions," *Phys. Chem. Chem. Phys.*, vol. 5, no. 16, pp. 3518–3524, 2003, doi: 10.1039/b306988p.

[11] J. Nordstrom, A. Sundblom, G. V. Jensen, J. S. Pedersen, A. Palmqvist, and A. Matic, "Silica/alkali ratio dependence of the microscopic structure of sodium silicate solutions," *J. Colloid Interface Sci.*, vol. 397, pp. 9–17, May 2013, doi: 10.1016/j.jcis.2013.01.048.

[12] R. V. Nauman and P. Debye, "Light-scattering investigations of carefully filtered sodium silicate solutions," *J. Phys. Colloid Chem.*, vol. 55, no. 1, pp. 1–9, Jan. 1951.

[13] E. Schaer, *Conception d'un procédé pour la production de microparticules filtrables et redispersables*. Vandoeuvre-les-Nancy, INPL, 1997.

[14] R. K. Iler, *The Chemistry of Silica: Solubility, Polymerization, Colloid and Surface Properties and Biochemistry of Silica*. New York: Wiley-Interscience, 1979.

[15] D. J. Belton, O. Deschaume, and C. C. Perry, "An overview of the fundamentals of the chemistry of silica with relevance to biosilicification and technological advances," *FEBS J.*, vol. 279, no. 10, pp. 1710–1720, mai 2012, doi: 10.1111/j.1742-4658.2012.08531.x.

[16] H. P. Rothbaum and A. G. Rohde, "Kinetics of silica polymerization and deposition from dilute solutions between 5 and 180°C," *J. Colloid Interface Sci.*, vol. 71, no. 3, pp. 533–559, Oct. 1979, doi: 10.1016/0021-9797(79)90328-X.

[17] S. Kitahara, "The polymerization of silicic acid obtained by the hydrothermal treatment of quartz and the solubility of amorphous silica," *Rev Phys Chem Jpn.*, vol. 30, pp. 131–137, 1960.

[18] D. J. Belton, O. Deschaume, S. V. Patwardhan, and C. C. Perry, "A solution study of silica condensation and speciation with relevance to in vitro investigations of biosilicification., A Solution Study of Silica Condensation and Speciation With relevance to in vitro investigations of biosilicification," *J. Phys. Chem. B J. Phys. Chem. B*, vol. 114, 114, no. 31, 31, pp. 9947, 9947–9955, Aug. 2010, doi: 10.1021/jp101347q, 10.1021/jp101347q.

[19] H. P. Rothbaum and R. D. Wilson, "Effect of temperature and concentration on the rate of polymerisation of silica in geothermal waters," *Geochemistry*, vol. 218, pp. 37–43, 1977.

[20] K. Goto, "Effect of pH on Polymerization of Silicic Acid," *J. Phys. Chem.*, vol. 60, no. 7, pp. 1007–1008, juillet 1956, doi: 10.1021/j150541a046.

[21] G. Okamoto, T. Okura, and K. Goto, "Properties of silica in water," *Geochim. Cosmochim. Acta*, vol. 12, no. 1–2, pp. 123–132, 1957.

[22] H. Baumann, "Polymerisation und Depolymerisation der Kieselsäure unter verschiedenen Bedingungen," *Colloid Polym. Sci. - COLLOID POLYM SCI*, vol. 162, pp. 28–35, 1959, doi: 10.1007/BF01513071.

[23] G. A. Icopini, S. L. Brantley, and P. J. Heaney, "Kinetics of silica oligomerization and nanocolloid formation as a function of pH and ionic strength at 25°C," *Geochim. Cosmochim. Acta*, vol. 69, no. 2, pp. 293–303, Jan. 2005, doi: 10.1016/j.gca.2004.06.038.

[24] A. D. Bishop and J. L. Bear, "The thermodynamics and kinetics of the polymerization of silicic acid in dilute aqueous solution," *Thermochim. Acta*, vol. 3, no. 5, pp. 399–409, Mar. 1972, doi: 10.1016/0040-6031(72)87054-0.

[25] S. H. Garofalini and H. Melman, "Applications of Molecular Dynamics Simulations to Sol-Gel Processing," *MRS Online Proc. Libr. Arch.*, vol. 73, Jan. 1986, doi: 10.1557/PROC-73-497.

[26] B. P. Feuston and S. H. Garofalini, "Onset of polymerization in silica sols," *Chem. Phys. Lett.*, vol. 170, no. 2–3, pp. 264–270, Jul. 1990, doi: 10.1016/0009-2614(90)87126-C.

[27] G. E. Martin and S. H. Garofalini, "Sol-gel polymerization: analysis of molecular mechanisms and the effect of hydrogen," *J. Non-Cryst. Solids*, vol. 171, no. 1, pp. 68–79, Jul. 1994, doi: 10.1016/0022-3093(94)90033-7.

[28] N. Z. Rao and L. D. Gelb, "Molecular Dynamics Simulations of the Polymerization of Aqueous Silicic Acid and Analysis of the Effects of Concentration on Silica Polymorph Distributions, Growth Mechanisms, and Reaction Kinetics," *J. Phys. Chem. B*, vol. 108, no. 33, pp. 12418–12428, Aug. 2004, doi: 10.1021/jp049169f.

[29] T. T. Trinh, A. P. J. Jansen, R. A. van Santen, and E. J. Meijer, "The role of water in silicate oligomerization reaction," *Phys. Chem. Chem. Phys.*, vol. 11, no. 25, pp. 5092–5099, 2009, doi: 10.1039/b819817a.

[30] A. Pavlova, T. T. Trinh, R. A. van Santen, and E. J. Meijer, "Clarifying the role of sodium in the silica oligomerization reaction," *Phys. Chem. Chem. Phys.*, vol. 15, no. 4, pp. 1123–1129, 2013, doi: 10.1039/c2cp42436c.

[31] A. C. T. van Duin, S. Dasgupta, F. Lorant, and W. A. Goddard, "ReaxFF: A Reactive Force Field for Hydrocarbons," *J. Phys. Chem. A*, vol. 105, no. 41, pp. 9396–9409, Oct. 2001, doi: 10.1021/jp004368u.

[32] Z. Jing, L. Xin, and H. Sun, "Replica exchange reactive molecular dynamics simulations of initial reactions in zeolite synthesis," *Phys. Chem. Chem. Phys.*, vol. 17, no. 38, pp. 25421–25428, 2015, doi: 10.1039/c5cp03063c.

[33] T. Du, H. Li, G. Sant, and M. Bauchy, "New insights into the sol-gel condensation of silica by reactive molecular dynamics simulations," *J. Chem. Phys.*, vol. 148, no. 23, p. 234504, Jun. 2018, doi: 10.1063/1.5027583.

[34] J. C. Fogarty, H. M. Aktulga, A. Y. Grama, A. C. T. van Duin, and S. A. Pandit, "A reactive molecular dynamics simulation of the silica-water interface," *J. Chem. Phys.*, vol. 132, no. 17, p. 174704, May 2010, doi: 10.1063/1.3407433.

[35] J. Yeon and A. C. T. van Duin, "ReaxFF Molecular Dynamics Simulations of Hydroxylation Kinetics for Amorphous and Nano-Silica Structure, and Its Relations with Atomic Strain

Energy," *J. Phys. Chem. C*, vol. 120, no. 1, pp. 305–317, Jan. 2016, doi: 10.1021/acs.jpcc.5b09784.

[36] K. Chenoweth, A. C. T. van Duin, and W. A. Goddard, "ReaxFF Reactive Force Field for Molecular Dynamics Simulations of Hydrocarbon Oxidation," *J. Phys. Chem. A*, vol. 112, no. 5, pp. 1040–1053, février 2008, doi: 10.1021/jp709896w.

[37] *ReaxFF*. SCM, Theoretical Chemistry, Vrije Universiteit, Amsterdam, The Netherlands, http://www.scm.com.

[38] A. Rahnamoun and A. C. T. van Duin, "Reactive Molecular Dynamics Simulation on the Disintegration of Kapton, POSS Polyimide, Amorphous Silica, and Teflon during Atomic Oxygen Impact Using the Reaxff Reactive Force-Field Method," *J. Phys. Chem. A*, vol. 118, no. 15, pp. 2780–2787, avril 2014, doi: 10.1021/jp4121029.

[39] Xueqing Zhang, "Kinetic Monte Carlo Modelling of The Initial Stages of Zeolite Synthesis," Eindhoven University of Technology, Eindhoven, 2012.

[40] H. Eyring, "The Activated Complex in Chemical Reactions," *J. Chem. Phys.*, vol. 3, no. 2, pp. 107–115, Feb. 1935, doi: 10.1063/1.1749604.

[41] M. V. Smoluchowski, "Drei Vortrage uber Diffusion, Brownsche Bewegung und Koagulation von Kolloidteilchen," *Z. Phys.*, vol. 17, pp. 557–585, 1916.

[42] A. V. Plyasunov, "Thermodynamic properties of H4SiO4 in the ideal gas state as evaluated from experimental data," *Geochim. Cosmochim. Acta*, 2011, Accessed: Jun. 23, 2020. [Online]. Available: https://agris.fao.org/agris-search/search.do?recordID=US201500113603.

[43] R. B. Bird, W. E. Stewart, and E. N. Lightfoot, "Transport Phenomena", John Wiley and Sons, Inc., New York (1960).

List of Tables

Table 5. The list of species detected at different time instants.

n_{HS}	T [K]	t_s [ns]	Detected species	The structure of randomly chosen cluster ($Si_{1>1}$)
1	300	0.003	51xSi_1, 2xSi_2, 3xSi_3 (N_0=64)	**Si_2**: $[Si(OH)_3O^-]_2[Na^+]_2$ **Si_3**: $[Si(OH)_3O^-]_3[Na^+]_3$
		0.15	38xSi_1, 1xSi_2, 4xSi_3, 1xSi_4, 1xSi_8 (N_0=64)	**Si_2**: $[Si(OH)_3O^-]_2[Na^+]_2$ **Si_3:** $[Si(OH)_3O^-]_2[Na^+]_2[(HO)Si(OH)_3]$ **Si_4** : $[Si(OH)_3O^-]_4[Na^+]_4[NaOH]$
	600	0.012	37xSi_1, 6xSi_2, 2xSi_3, 1xSi_4, 1xSi_5 (N_0=64)	**Si_5**: $[Si(OH)_3O^-]_5[Na^+]_5[H_2O]$
		0.10	49xSi_1, 1xSi_2, 1xSi_{13} (N_0=64)	**Si_2**: $[Si(OH)_3O^-]_2[Na^+]$. **Si_{13}**: sodium atoms creating a net-like structure
	1000	0.15	46xSi_1, 1xSi_3, 2xSi_4, 1xSi_7 (N_0=64)	**Si_7**: $[Si(OH)_3O^-]_3[Si(OH)_2(ONa)O^-]_2[SiO_4^{4-}]$ $[Si(OH)O_3^{3-}][Na^+]_{13}[NaOH]$
	1500	0.15	47xSi_1, 5xSi_2, 1xSi_3, 1xSi_4 (N_0=64)	**Si_2**: $[Si(OH)_3O^-][Si(OH)(ONa)_2O^-][Na^+]_3$ **Si_4**: $[Si(OH)_3O^-]_2[Si(OH)_2(ONa)O^-]_2[Na^+]_2$
		0.35	48xSi_1, 5xSi_2, 1xSi_6 (N_0=64)	**Si_6** (covalent bond)**:** $[Si(OH)_3O^-][Si(OH)_2(ONa)O^-][Si_2O_7H_5^-]_2[Na^+]_5$
	2000	0.10	56xSi_1, 2xSi_2, 1xSi_4 (N_0=64)	**Si_2**: $[Si(OH)_3O^-]_2[Na^+]$ **Si_2**: $[Si(OH)_3O^-][Si(OH)_2(ONa)O^-][Na^+]$ **Si_4**: $[Si(OH)_3O^-]_2[Si(OH)_2(ONa)O^-]$ $[Si(OH)(ONa)O_2^{2-}][Na^+]_3[NaOH]$
0	1500	0.15	47xSi_1, 6xSi_2, 1xSi_5 (N_0=64)	**Si_5**: $[Si(OH)_3O^-]_3[Si(OH)_2(ONa)O^-]$ $[Si(OH)_2O_2^{2-}][Na^+]_5$
2	1500	0.15	56xSi_1, 4xSi_2, 1xSi_4 (N_0=68)	**Si_4:** $[Si(OH)_3O^-]_3[Si(OH)_2O_2^{2-}]$ $[Na^+]_5$

Table 6. The values of the molar fractions of species, $x_{N=1-4}$, coexisting in equilibrium.

T [K]	$\mathbf{x_1}$	$\mathbf{x_2}$	$\mathbf{x_3}$	$\mathbf{x_4}$
600	0.75	0.015	0.006	0.003
1000	0.75	0.022	0.01	0.005

Table 7. The list of kinetic constants estimated for different T, N_0, and n_{HS}.

N_0	n_{HS}	$k_{1,dir}$ [1/ns]	$k_{2,dir}$ [1/ns]	$k_{3,dir}$ [1/ns]	$k_{1,rev}$ [1/ns]	$k_{2,rev}$ [1/ns]	$k_{3,rev}$ [1/ns]	k_4 [1/ns]	k_5 [1/ns]	$k_{6,dir}$ [1/ns]	$k_{6,rev}$ [1/ns]	k_7 [1/ns]	err
T=300K													
64	0	171	210	149	102	100	45	16	16	216	61	0	0.0164
64	0.5	233	270	89	164	113	64	17	13	317	50	0	0.0174
64	1	227	290	293	140	126	89	17	13	328	72	0	0.0165
68	2	249	271	333	141	93	95	16	18	208	81	0	0.0104
216	0	360	281	246	154	117	118	14	18	364	81	0	0.0082
216	1	343	251	186	135	86	47	14	15	162	49	0	0.0065
T=600K													
64	0	345	290	203	41	118	41	888	761	212	145	0	0.0095
64	0.5	347	122	139	52	150	95	908	881	214	113	0	0.0099
64	1	329	104	178	42	127	73	850	839	187	181	0	0.0110
68	2	370	220	228	60	159	68	904	762	126	133	0	0.0103
216	0	342	170	161	42	120	106	823	833	308	122	0	0.0055
216	1	361	279	307	54	147	113	901	648	137	119	0	0.0054
T=1000K													
64	0	318	206	120	171	151	71	625	647	135	178	0	0.0161
64	0.5	292	206	192	177	137	100	452	922	141	138	0	0.0129
64	1	314	232	267	135	130	162	302	874	118	154	0	0.0130
68	2	308	161	288	84	135	74	638	754	105	171	0	0.0100
216	0	356	161	131	80	119	101	646	867	133	153	0	0.0085
216	1	369	188	191	54	146	82	785	838	118	119	0	0.0099
T=1500K													
64	0	104	104	225	175	113	129	2.5	3.2	163	104	0.1	0.0210
64	0.5	84	164	166	181	168	87	2.5	1.8	283	170	0.1	0.0171
64	1	101	152	233	179	163	157	2.6	1.4	209	120	0.1	0.0129
68	2	96	113	126	176	158	70	0.9	1.6	113	109	0.1	0.0151

N_0	n_{HS}	$k_{1,dir}$ [1/ns]	$k_{2,dir}$ [1/ns]	$k_{3,dir}$ [1/ns]	$k_{1,rev}$ [1/ns]	$k_{2,rev}$ [1/ns]	$k_{3,rev}$ [1/ns]	k_4 [1/ns]	k_5 [1/ns]	$k_{6,dir}$ [1/ns]	$k_{6,rev}$ [1/ns]	k_7 [1/ns]	err
216	0	138	117	80	185	179	160	1.6	3.0	235	88	0.1	0.0222
216	1	80	138	97	185	170	52	1.0	1.6	98	99	0.1	0.0163
T=2000K													
64	0	185	102	147	176	100	111	2.6	2.7	96	108	0.1	0.0204
64	0.5	90	118	127	170	145	100	3	1.7	126	73	5	0.0206
64	1	79	105	122	174	153	170	1.5	2.7	102	83	7	0.0170

Table 8. The list of kinetic constants, k_0, estimated for the collisions of small species based on Eyring's diffusion-aggregation theory.

T [K]	**$k_0(Si_1+Si_1)$** [1/ns]	**$k_0(Si_1+Si_2)$** [1/ns]	**$k_0(Si_1+Si_3)$** [1/ns]
300	800	769	768
1000	1455	1404	1402

List of Figures

Figure 8. The MD-derived evolution of species corrected to account for the conservation of the mass compared to the evolution of species calculated from our simplified model for three temperatures. nHS=1; MD-derived data – dashed lines, estimated data – solid line; Si1 - black, Si2 - red, Si3 - blue, Si4 – magenta.

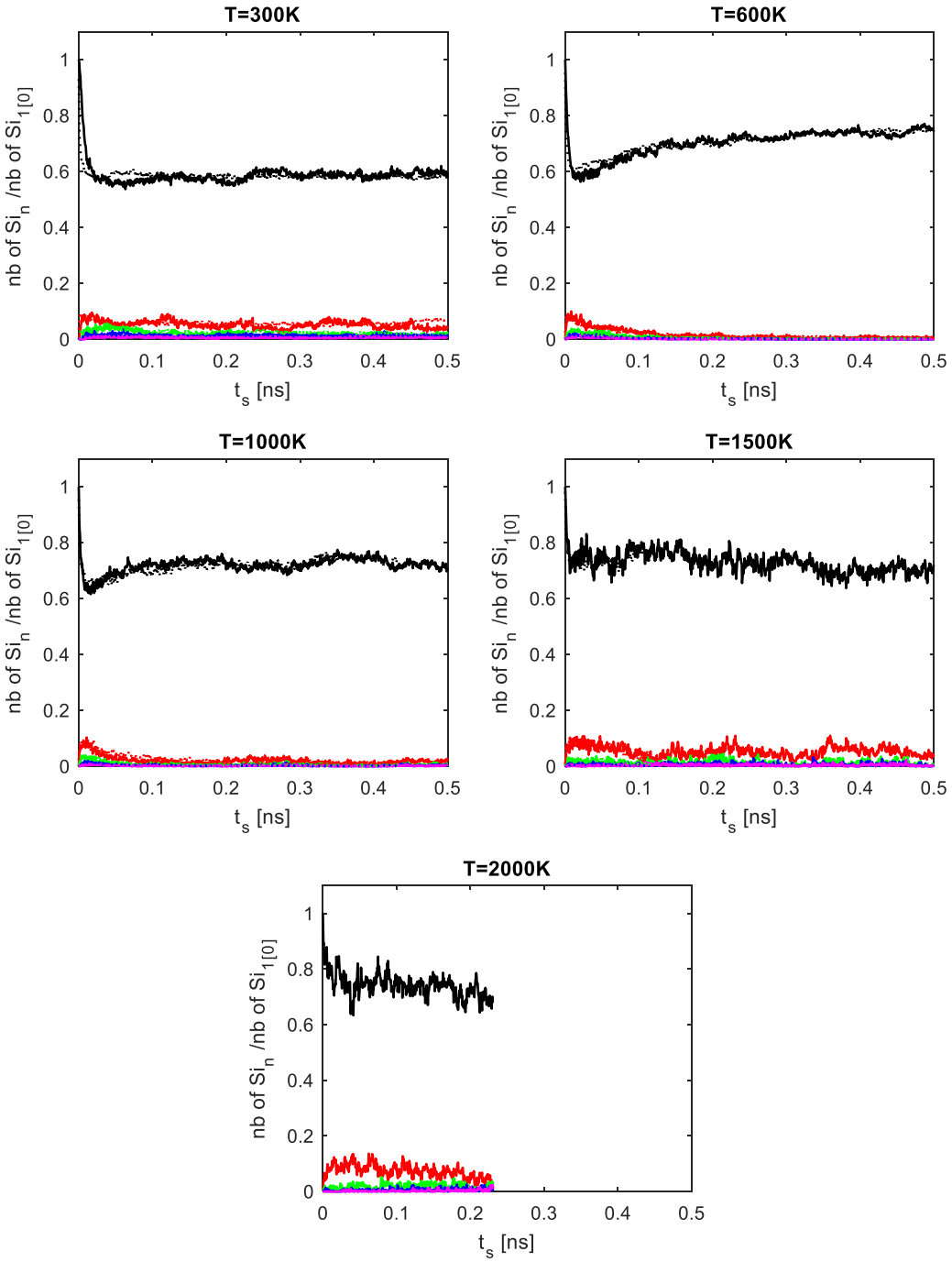

Figure 1. The effect of N_0 and T on the temporal evolution of species (Si_1 to Si_4 for the clarity purposes) for the systems with N_0=64 as compared to N_0=216 at T=300, 600, 1000, 1500 and 2000K; n_{HS}=0; N_0=64 - solid line, N_0=216 - dotted line; Si_1 - black, Si_2 - red, Si_3 - blue, Si_4 - magenta. Simulations for N_0=216 at T=1500K and N_0=64 at 2000K stopped prematurely. At 2000K, we did not get exploitable results for N_0=216.

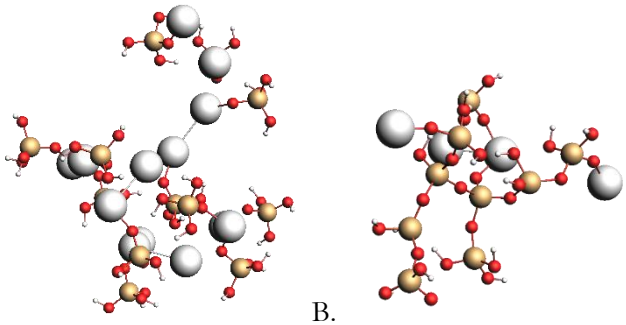

A. B.

Figure 2. Examples of species detected in the presence of Na^+ ions for C_0 =342gSiO_2/L at 300K – Si_{12} (A) and 2000K – Si_9 (B).

Si: yellow; O: red; Na: gray

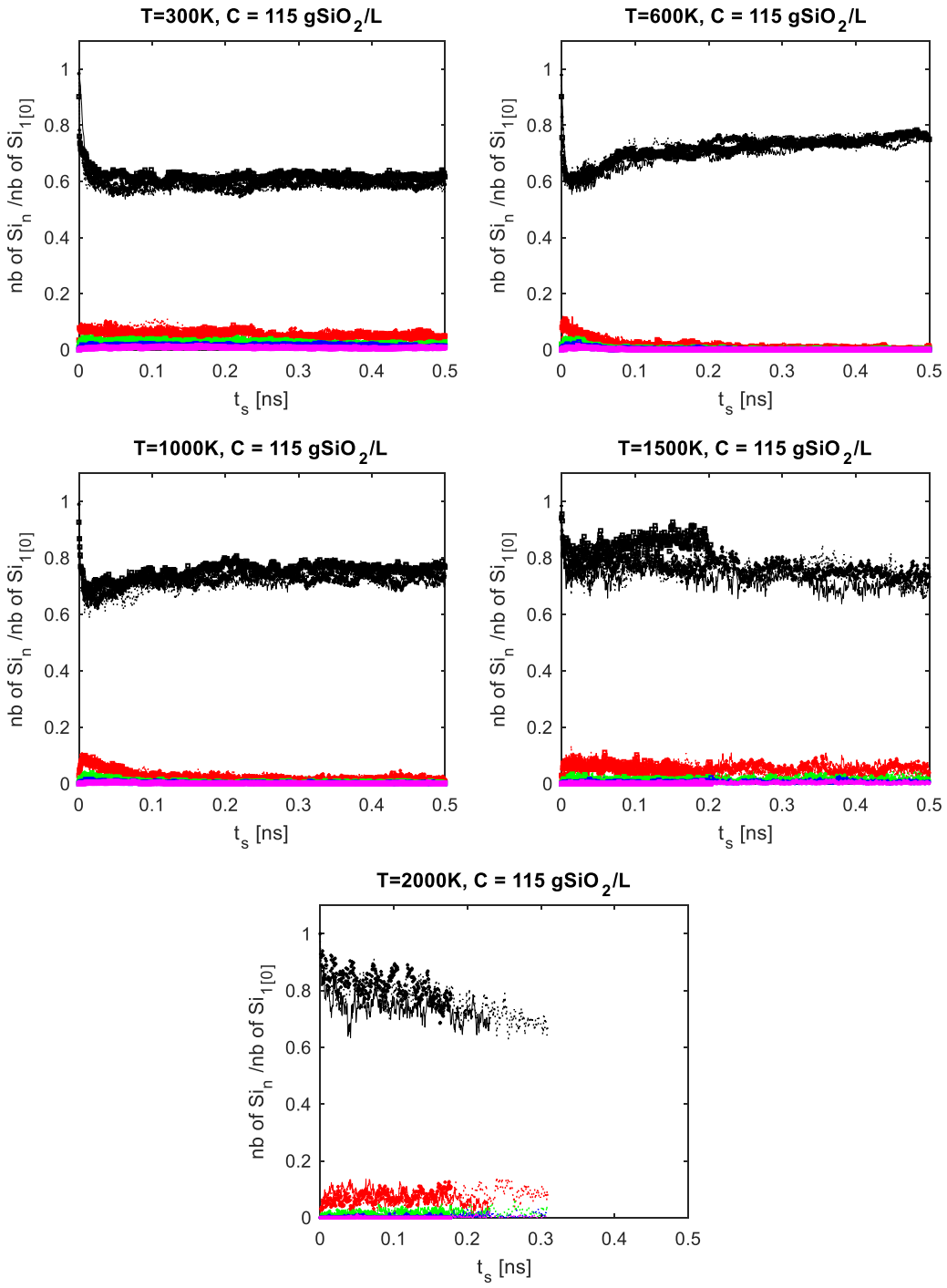

Figure 3. The effect of n_{HS} and T on the temporal evolution of species (Si_1 to Si_4 for the clarity purposes) for the systems with n_{HS}=0, 0.5, 1, and 2 at T=300, 600, 1000, 1500 and 2000K; N_0=64/68; n_{HS}=0 - solid line, n_{HS}=0.5 - dotted line, n_{HS}=1 - cross, n_{HS}=2 - square; Si_1 - black, Si_2 - red, Si_3 - blue, Si_4 - magenta; Simulations at T=1500K stopped prematurely for n_{HS}=2, at 2000K for n_{HS}=0, 0.5, 1. At 2000K, we did not get exploitable results for n_{HS}=2.

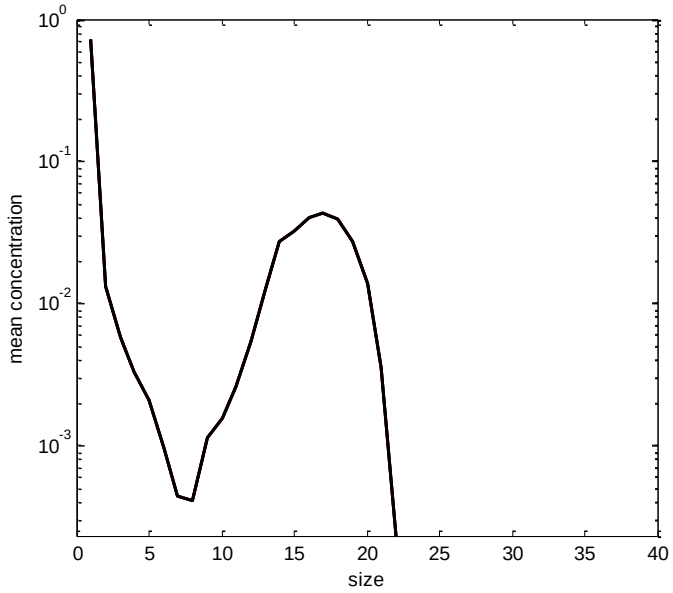

Figure 4. Mass-based particle size distribution; n_{HS}=1, T=600K, t_s=0.174ns.

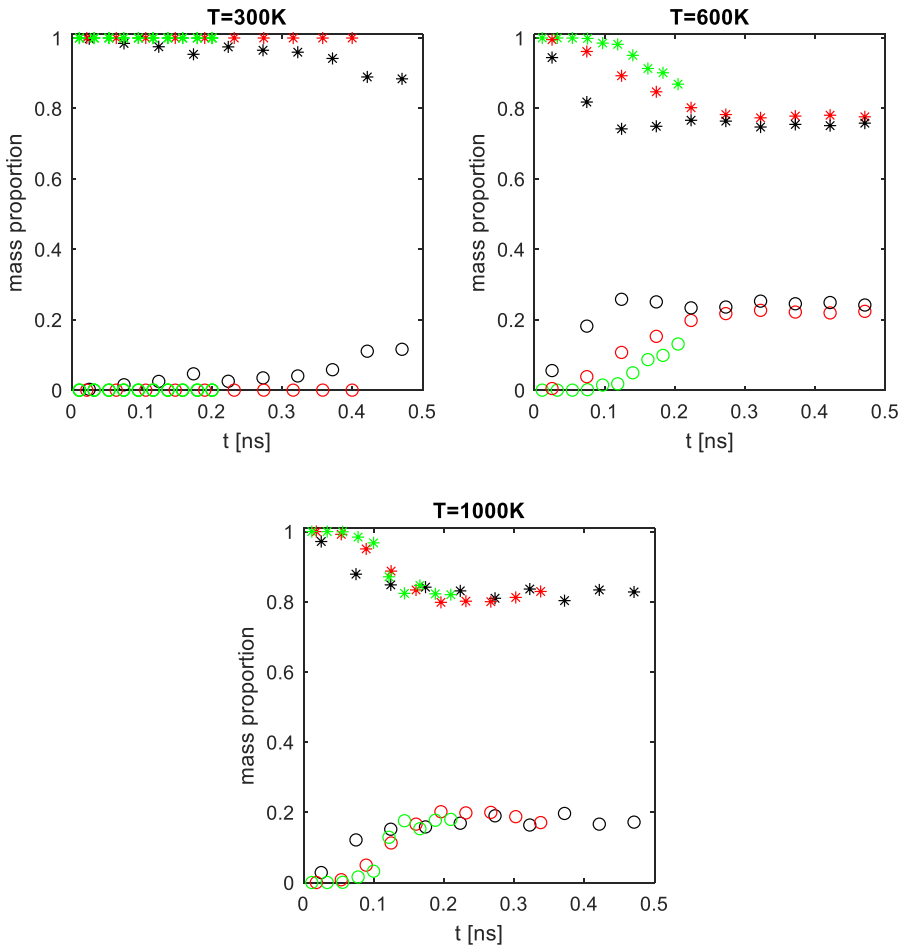

Figure 5. The effect of N_0 and T on the temporal evolution of the mass proportion of the large clusters ($N>N_0/8$) and smaller clusters ($N\leq N_0/8$); $n_{HS}=1$, $C_0=115 gSiO_2/L$;
smaller clusters - stars, larger clusters – circles; $N_0=500$ – green, $N_0=216$ – red, $N_0=64$ – black.

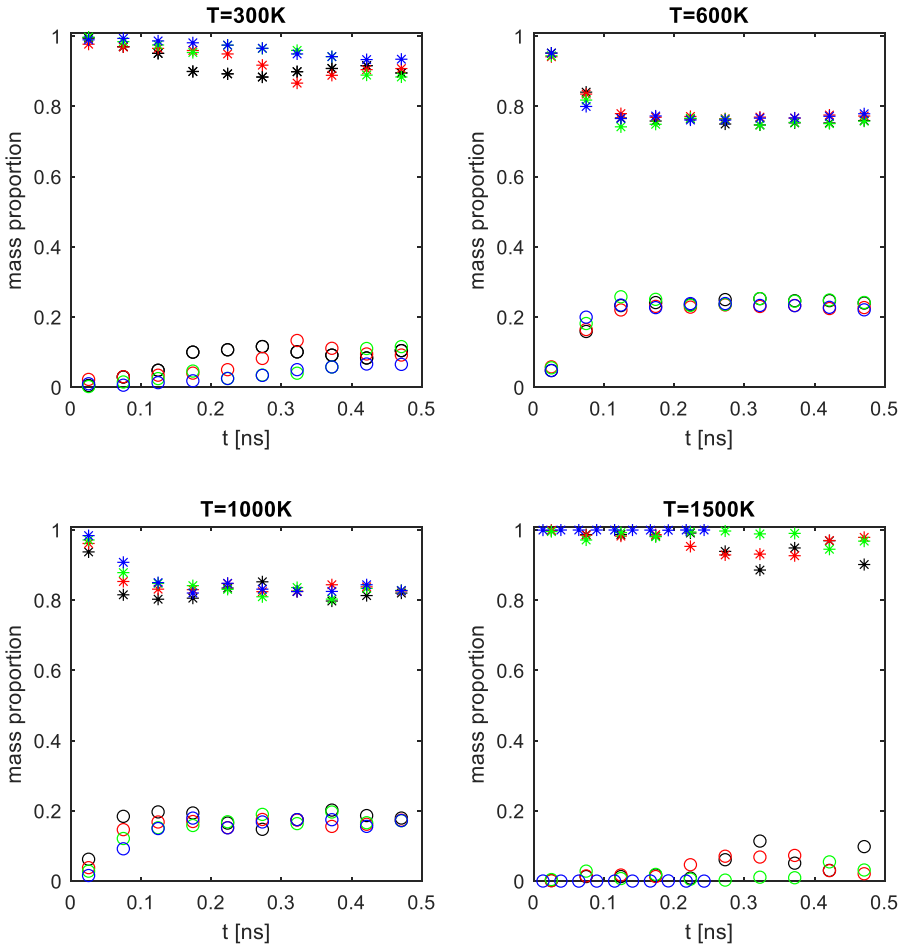

Figure 6. The effect of n_{HS} and T on the temporal evolution of the mass proportion of the large clusters ($N>N_0/8$) and smaller clusters ($N\leq N_0/8$); $N_0=64$, $C_0=115 gSiO_2/L$;
smaller clusters - stars, larger clusters – circles;
$n_{HS}=0$- black, $n_{HS}=0.5$- red, $n_{HS}=1$- green, $n_{HS}=2$-blue.

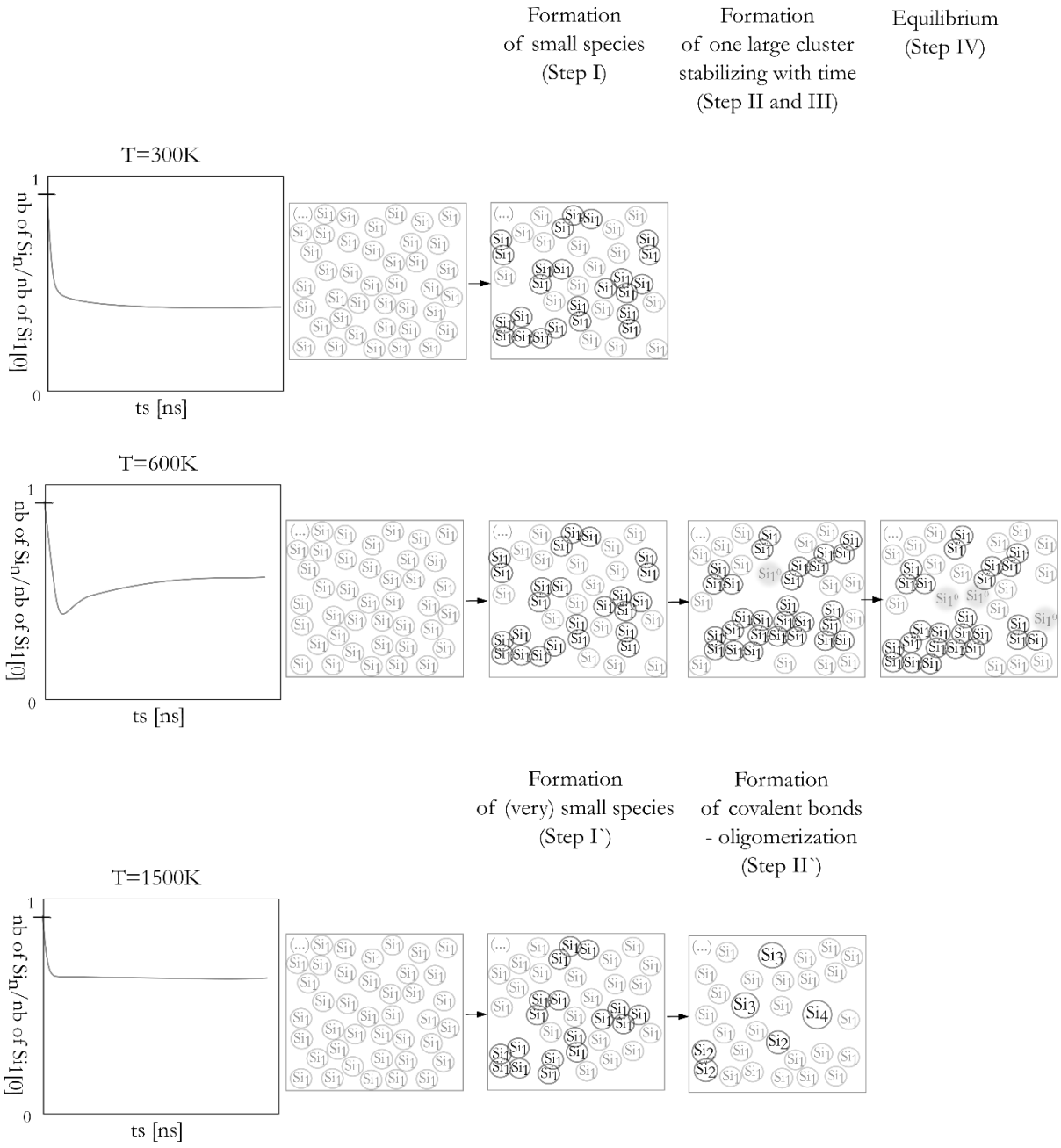

Figure 7. A schematic representation of the reaction mechanism at different temperatures; For clarity reasons, we included the non-reactive neutral monomer (Si_1^0) only as a product of the internal reorganization reaction.

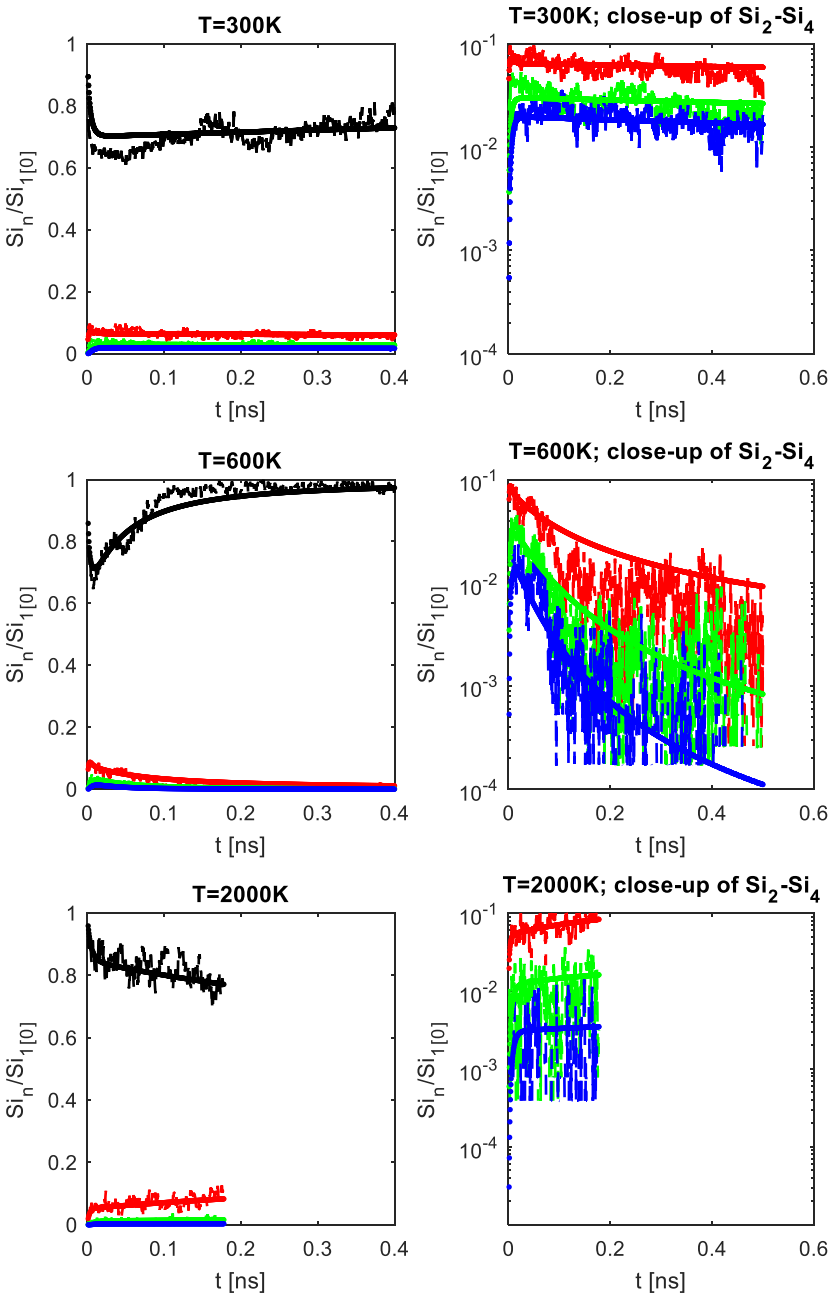

Figure 8. The MD-derived evolution of species corrected to account for the conservation of the mass compared to the evolution of species calculated from our simplified model for three temperatures. n_{HS}=1; MD-derived data – dashed lines, estimated data – solid line; Si_1 - black, Si_2 - red, Si_3 - blue, Si_4 – magenta.